Extracting equations of motion from superconducting circuits

Christian Z. Pratt ⊙,* Kyle J. Ray ⊙,† and James P. Crutchfield ⊙‡

Complexity Sciences Center and Department of Physics and Astronomy, University of California, Davis, Davis, California 95616, USA

Alternative computing paradigms open the door to exploiting recent innovations in computational hardware to probe the fundamental thermodynamic limits of information processing. One such paradigm employs superconducting quantum interference devices (SQUIDs) to execute classical computations. This, though, requires constructing sufficiently complex superconducting circuits that support a suite of useful information processing tasks and storage operations, as well as understanding these circuits' energetics. First-principles circuit design leads to prohibitive algebraic complications when deriving the effective equations of motion—complications that to date have precluded achieving these goals, let alone doing so efficiently. We circumvent these complications by (i) specializing our class of circuits and physical operating regimes, (ii) synthesizing existing derivation techniques to suit these specializations, and (iii) implementing solution-finding optimizations which facilitate physically interpreting circuit degrees of freedom that respect physically grounded constraints. This leads to efficient and practical circuit prototyping, as well as accessing scalable circuit architectures. The analytical efficiency is demonstrated by reproducing the potential energy landscape generated by a SQUID. We then show how inductively coupling two SQUIDs produces a device that is capable of executing two-bit computations via its composite potential energy landscape. More generally, the synthesized methods detailed here provide a basis for constructing universal logic gates and investigating their thermodynamic performance.

I. INTRODUCTION

All computation is physical. To effect information processing, one approach entails a sequence of stochastic transformations that systematically manipulate a system's potential energy landscape [1,2]. Reliable computing, in particular, then requires stable memory states physically supported by a system's information-bearing degrees of freedom [3]. Energy minima on the landscape provide this dynamical stability. Computation, then, consists of externally controlling the creation, destruction, and location of energy minima. From this perspective, a device's time-dependent potential energy surface guides the emergence of its computational capabilities.

Exploring a superconducting circuit's ability to perform computational operations in this way involves understanding the device's energetics and subsequent dynamical equations of motion [4–8]. Success in using this approach to design candidate devices, though, requires rapidly determining if a given circuit construction is capable of carrying out computations. This requirement demands a framework that can efficiently derive a circuit's equations of motion. To accomplish this, we

synthesize several previous approaches, specializing them to a class of circuits of practical interest. The result is a methodology for generating a readily interpretable Lagrangian and associated equations of motion for a given circuit in terms of its classical degrees of freedom.

The framework's success is demonstrated through two examples. First, we efficiently reproduce the Lagrangian of a superconducting quantum interference device (SQUID) [4,5,9–11], which has been used to perform one-bit computations [3,9,12–14], in Sec. IV A. Then we derive the circuit Lagrangian of a device created by inductively coupling two SQUIDs in Sec. IV B; the device can be used to execute a range of two-bit classical computations. We outline how computations are carried out with these devices in the Appendix.

II. RELATED WORK

The following synthesizes methods from Refs. [15–18]; its foundations build on Refs. [15,16], which introduced a network-theoretic approach to electrical circuit analysis. This approach is advantageous because solely using Kirchoff's laws becomes more inconvenient and cumbersome as the number of components and loops in a circuit increases [19]. Further advancing the network theory approach to avoid these complications, Ref. [17] introduced an elegant technique for multiloop circuits to find *irrotational* degrees of freedom by rotating into a reference frame that can simplify a given circuit's behavior; this method has recently been experimentally verified [20]. However, it considered only the circuit's quantum Hamiltonian for investigating time-dependent quantities, such as the transition probabilities between energy eigen-

---

*Contact author: czpratt@ucdavis.edu
†Contact author: kjray@ucdavis.edu
‡Contact author: chaos@ucdavis.edu

states. This departs from our goals. Additionally, Ref. [17] restricted each circuit loop to have at most one inductor: If this condition is not met, then Ref. [17] finds a continuum of coordinate rotations that can be accessed. In the following we eschew this restriction and investigate circuits that contain more than one inductor in a loop. To address the continuum of possible rotations, we establish guidelines for finding suitable coordinate rotations and eliminate cyclic degrees of freedom after the circuit Lagrangian is obtained.

Here we use the resistive capacitive shunted junction (RCSJ) model for each Josephson junction (JJ). Due to this, the dissipative dynamics arising from finite-valued direct current (dc) resistances must be accounted for. To do this, we rely on Ref. [18]'s method that uses the Rayleigh dissipation function [21] to model the circuit's resistive shunts.

Several alternative approaches are available to analyze circuit behaviors in the quantum regime. One such procedure employs number-phase quantization [22,23], which does not use a network-theoretic approach. Simulations of the quantum dynamics of similar circuits are detailed in Ref. [24]. This all noted, though the SQUIDs employed here are often the basis for quantum computing devices, we concentrate on their behavior in the classical regime to understand their information-bearing degrees of freedom [10,12]. This also greatly facilitates follow-on investigations of their far-from-equilibrium thermodynamic performance. An alternative approach to superconducting circuit analysis with magnetic flux is to consider charge in a loop [25]. However, previous works [12,15,17,26] showed that considering magnetic flux provides more convenience for circuit control analysis. Due to this, we ground this work in a flux-focused interpretation. A generalized approach to the techniques implemented in Ref. [17] considers arbitrary circuit geometries and electromagnetic fields to construct a Hamiltonian [27]. However, the goal of this work is to advance the network-theoretic approach to superconducting circuits taken by Refs. [15–18] to rapidly and directly characterize candidate superconducting circuit designs. Due to this, a first-principles framework will not be employed here.

III. SUPERCONDUCTING CIRCUIT ANALYSIS

First, we obtain the equations of motion for a given circuit. Then, we show how to find coordinate transformations that produce readily interpretable equations of motion in Langevin form.

A. Circuit equations of motion

Following Ref. [15], we define a *branch* to be a particular circuit element, whose time-dependent *branch flux* is defined by:

$$\phi_b = \phi_b(t)$$
$$:= \int_{-\infty}^{t} dt' \, v_b(t').$$

This is related to the branch voltage $v_b(t)$, the instantaneous voltage across the circuit element, and the *reduced branch flux* $\varphi_b = 2\pi\phi_b/\Phi_0$, where Φ_0 is the flux quantum.

Before proceeding, several assumptions need to be addressed. To begin, all branches within a circuit correspond to either a JJ or an inductor. Corresponding variables are subscripted with a J or L, respectively. All JJs are described by the RCSJ model [28,29], which is characterized by a critical current I_c [7], capacitance C_J, and dc resistance R. Following Refs. [15,17,19], each inductive branch is modeled by an inductance L in parallel with a parasitic capacitance C_L.

Suppose a circuit is constructed with n JJs and m inductors for a total of $N = n + m$ branches. The *branch flux* vector $\mathbf{\Phi}_b := (\phi_{J_1} \cdots \phi_{J_n}\phi_{L_1} \cdots \phi_{L_m})^\mathsf{T}$ compactly represents all circuit branch fluxes. When computing the potential and equations of motion, we refer to the *truncated branch flux* vectors $\mathbf{\Phi}_{b_J} := (\phi_{J_1} \cdots \phi_{J_n})^\mathsf{T}$ and $\mathbf{\Phi}_{b_L} := (\phi_{L_1} \cdots \phi_{L_m})^\mathsf{T}$.

The energy stored in the capacitive components is [15]

$$\mathcal{L}_T = \tfrac{1}{2}\dot{\mathbf{\Phi}}_b^\mathsf{T}\mathbf{C}\dot{\mathbf{\Phi}}_b, \tag{1}$$

where the overdot (˙) indicates a time derivative and the *capacitance* matrix is written as:

$$\mathbf{C} = \begin{pmatrix} C_{J_1} & \cdots & C_{J_1 J_n} & C_{J_1 L_1} & \cdots & C_{J_1 L_m} \\ \vdots & \ddots & \vdots & \vdots & \vdots & \vdots \\ C_{J_n J_1} & \cdots & C_{J_n} & C_{J_n L_1} & \cdots & C_{J_n L_m} \\ C_{L_1 J_1} & \cdots & C_{L_1 J_n} & C_{L_1} & \cdots & C_{L_1 L_m} \\ \vdots & \vdots & \vdots & \vdots & \ddots & \vdots \\ C_{L_m J_1} & \cdots & \cdots & \cdots & \cdots & C_{L_m} \end{pmatrix}. \tag{2}$$

Here C_{p_i} represents the self-capacitance of component p of index i, while $C_{p_i q_j}$ represents the cross-capacitance between p_i and another component q of index j, all for $p, q \in \{J, L\}$ with $p \neq q$ and $j \neq i$. This said, we assume that all cross-capacitances are negligible, resulting in all nondiagonal elements being zero valued. Following Ref. [17], we assume that the parasitic capacitance of the inductive branches C_L to be vanishingly small, and we keep C_L as an auxiliary variable rather than setting it to zero to preserve the invertibility of $\mathbf{C}$. Nonideal branches can be taken into account in an experimental setting [19]; one way to do this is to instantiate nonzero values for C_L.

Together, this yields:

$$\mathbf{C} := \mathrm{diag}\,(C_{J_1}, \ldots, C_{J_n}, C_{L_1}, \ldots, C_{L_m}).$$

Since we assume that all branches are either inductors or JJs, the energy stored in the inductive elements can be calculated using only $\mathbf{\Phi}_{b_L}$. The $m \times m$ *inductance* matrix $\mathbf{L}$ denotes the circuit's linear inductances, with diagonal entries corresponding to self-inductances L_i and off-diagonal entries corresponding to the mutual inductive coupling $-M_{ij}$ between L_i and $L_{j\neq i}$. The energy stored in the inductive components is given by [15]:

$$\mathcal{L}_L = \tfrac{1}{2}\mathbf{\Phi}_{b_L}^\mathsf{T}\mathbf{L}^{-1}\mathbf{\Phi}_{b_L}. \tag{3}$$

Up to a constant, the JJ potential energy contribution is [15]

$$\mathcal{L}_J = -\sum_{i=1}^{n} E_i \cos\left(\frac{2\pi}{\Phi_0}\Phi_{b_J i}\right). \tag{4}$$

Here $E_i = I_{ci}(\Phi_0/2\pi)$ is the Josephson energy of the ith JJ in a circuit, which is further characterized by its critical current I_{ci}.

Equations (3) and (4) together give the circuit's conservative potential energy $\mathcal{L}_V := \mathcal{L}_J + \mathcal{L}_L$. Given a physical circuit consisting of inductors and JJs as described above, the circuit Lagrangian $\mathcal{L} := \mathcal{L}_T - \mathcal{L}_V$ is, up to a constant:

$$\mathcal{L} = \frac{1}{2}\dot{\boldsymbol{\Phi}}_b^{\mathsf{T}}\mathbf{C}\dot{\boldsymbol{\Phi}}_b - \frac{1}{2}\boldsymbol{\Phi}_{b_L}^{\mathsf{T}}\mathbf{L}^{-1}\boldsymbol{\Phi}_{b_L} + \sum_{i=1}^{n} E_i \cos\left(\frac{2\pi}{\Phi_0}\Phi_{b,i}\right). \tag{5}$$

The nonconservative dissipation from the finite JJ resistive shunts are taken into account by the Rayleigh dissipation function $\mathcal{D}$ and further incorporated into the Euler-Lagrange equations of motion [18,21] in terms of a generalized coordinate q_i, as:

$$\frac{d}{dt}\frac{\partial \mathcal{L}}{\partial \dot{q}_i} = \frac{\partial \mathcal{L}}{\partial q_i} - \frac{\partial \mathcal{D}}{\partial \dot{q}_i}, \tag{6}$$

with

$$\mathcal{D} := \sum_{i=1}^{n}\frac{1}{2R_i}(\dot{\phi}_{J_i})^2. \tag{7}$$

$\mathcal{D}$ accounts for the dissipated power in each JJ branch due to its shunt resistance R_i in terms of its branch flux ϕ_{J_i}. To obtain this relation in matrix form, we first let:

$$\mathbf{D} = \mathrm{diag}(R_{J_1}, \dots, R_{J_n}).$$

Then, the dissipation function reads:

$$\mathcal{D} = \tfrac{1}{2}\dot{\boldsymbol{\Phi}}_{b_J}^{\mathsf{T}}\mathbf{D}^{-1}\dot{\boldsymbol{\Phi}}_{b_J}. \tag{8}$$

To conclude, we add the phenomenological contribution of the dc resistances' thermal noise current to the equations of motion via:

$$\frac{d}{dt}\frac{\partial \mathcal{L}}{\partial \dot{q}_i} = \frac{\partial \mathcal{L}}{\partial q_i} - \frac{\partial \mathcal{D}}{\partial \dot{q}_i} + \eta_i(t), \tag{9}$$

in which $\eta_i(t)$ is nonzero for the JJ branches only. One common method of modeling $\eta_i(t)$ is a Langevin treatment [10], in which we consider them to be statistically independent of each other, delta correlated over time, and determined by the fluctuation-dissipation theorem through the relation:

$$\langle \eta_i(t)\eta_j(t')\rangle = \frac{2k_B T}{R_i}\delta_{ij}\delta(t-t').$$

B. Determining interpretable coordinates

Despite the fact that Eq. (6) marginally accommodates the circuit's topology, it does not account for fluxoid quantization conditions [15,30]. These require that the sum of the branch fluxes around any loop equals the external flux threading the loop. As a result, while there may appear to be $N = n + m$ degrees of freedom in the Lagrangian, there are only $N - F$ degrees of freedom in a circuit with F independent loops—i.e., loops that contain no other loops—threaded by external fluxes.

In view of this, the *external flux vector* $\boldsymbol{\Phi}_x := (\phi_{x_1} \cdots \phi_{x_F})^{\mathsf{T}}$ is defined to cast fluxoid quantization into matrix form [17]:

$$\boldsymbol{\Phi}_x = \mathbf{R}\boldsymbol{\Phi}_b.$$

The $F \times N$ matrix $\mathbf{R}$ is constructed in such a way that its elements R_{ij} satisfy the following criteria: Let L_i denote the ith loop threaded by the external flux Φ_{xi} that may contain branch flux ϕ_j. Then:

$$R_{ij} := \begin{cases} +1 & \phi_j \in \mathsf{L}_i \text{ same orientation as } \Phi_{xi}, \\ -1 & \phi_j \in \mathsf{L}_i \text{ opposite orientation as } \Phi_{xi}, \text{ and} \\ 0 & \phi_j \notin \mathsf{L}_i. \end{cases}$$

Finally, the circuit's degrees of freedom are defined as $\widetilde{\boldsymbol{\Phi}} := (\tilde{\phi}_1 \cdots \tilde{\phi}_{N-F})^{\mathsf{T}}$ [17]. Generally, these are a to-be-determined linear combination of the branch fluxes represented by the $(N-F) \times N$ matrix $\mathbf{M}$:

$$\widetilde{\boldsymbol{\Phi}} = \mathbf{M}\boldsymbol{\Phi}_b.$$

Furthermore, due to fluxoid quantization, no more than $N - F$ degrees of freedom in the circuit are expected. The quantization conditions are included by employing the $N \times 1$ *augmented flux* vector $\widetilde{\boldsymbol{\Phi}}_+$ and the $N \times N$ *augmented* matrix $\mathbf{M}_+$ [17]:

$$\widetilde{\boldsymbol{\Phi}}_+ := \begin{pmatrix} \widetilde{\boldsymbol{\Phi}} \\ \boldsymbol{\Phi}_x \end{pmatrix},$$

$$\mathbf{M}_+ := \begin{pmatrix} \mathbf{M} \\ \mathbf{R} \end{pmatrix}.$$

Note that the branch flux vector and the augmented flux vector are directly related to each other through $\mathbf{M}_+$ by:

$$\widetilde{\boldsymbol{\Phi}}_+ = \mathbf{M}_+\boldsymbol{\Phi}_b. \tag{10}$$

With this, the circuit Lagrangian and associated equations of motion can be written in terms of $\widetilde{\boldsymbol{\Phi}}_+$ by substituting $\boldsymbol{\Phi}_b = \mathbf{M}_+^{-1}\widetilde{\boldsymbol{\Phi}}_+$ into Eq. (5) and Eq. (6), respectively. Specifically, to find the circuit's Lagrangian in terms of $\widetilde{\boldsymbol{\Phi}}_+$, $\mathbf{M}_+$ must be invertible. Provided that the columns of $\mathbf{M}$ are chosen to be linearly independent of each other and of the columns of $\mathbf{R}$, the nonsingularity of $\mathbf{M}_+$ is guaranteed.

However, ambiguity remains in defining the elements of $\mathbf{M}$. Following Ref. [17], these degrees of freedom are deemed *irrotational* by ensuring that they satisfy the following constraint:

$$\mathbf{R}\mathbf{C}^{-1}\mathbf{M}^{\mathsf{T}} = \mathbf{0}. \tag{11}$$

This guarantees that the Lagrangian, when written in terms of $\widetilde{\boldsymbol{\Phi}}_+$, does not depend on $\dot{\boldsymbol{\Phi}}_x$. Due to this, $\widetilde{\boldsymbol{\Phi}}$ is referred to as the *irrotational flux* vector, and $\widetilde{\boldsymbol{\Phi}}_+$ is the *augmented irrotational flux* vector. In addition, Eq. (11) allows the equations of

motion to be of Langevin form, further enabling thermodynamical analyses of the circuit's degrees of freedom—the subject of a sequel.

However, even after enforcing the irrotational constraint, there is still additional freedom in defining $\mathbf{M}$. To address this, we turn to the kinetic energy term:

$$\mathcal{L}_T = \tfrac{1}{2} \dot{\boldsymbol{\Phi}}_b^{\mathsf{T}} \mathbf{C} \dot{\boldsymbol{\Phi}}_b \tag{12}$$

$$= \tfrac{1}{2} \dot{\tilde{\boldsymbol{\Phi}}}_+^{\mathsf{T}} (\mathbf{M}_+^{-1})^{\mathsf{T}} \mathbf{C} \mathbf{M}_+^{-1} \dot{\tilde{\boldsymbol{\Phi}}}_+$$

$$= \tfrac{1}{2} \dot{\tilde{\boldsymbol{\Phi}}}_+^{\mathsf{T}} \mathbf{C}_{\mathrm{eff}} \dot{\tilde{\boldsymbol{\Phi}}}_+ \, , \tag{13}$$

in which $\mathbf{C}_{\mathrm{eff}}$ is the *effective capacitive* matrix. With Eq. (13) in mind, recall that the goal is to obtain an easily interpretable Lagrangian and corresponding equations of motion for a given circuit. A diagonal $\mathbf{C}_{\mathrm{eff}}$ allows for a straightforward interpretation of $\mathcal{L}_T$ as the kinetic energy in both the $\boldsymbol{\Phi}_b$ and the $\tilde{\boldsymbol{\Phi}}$ bases. In other words, the task is to find solutions of $\mathbf{M}$ that yield a diagonal $\mathbf{C}_{\mathrm{eff}}$.

We now present a set of guidelines for the elements of $\mathbf{M}$ that yield a diagonal $\mathbf{C}_{\mathrm{eff}}$. We note here that for circuits with more than one independent loop, these guidelines will yield a diagonal $\mathbf{C}_{\mathrm{eff}}$ only when $m \geqslant F$. After detailing these guidelines, we discuss their implications and explain how failing to satisfy $m \geqslant F$ leads to a nondiagonal $\mathbf{C}_{\mathrm{eff}}$—i.e., generating a less interpretable circuit Lagrangian and equations of motion.

(1) The first n rows of $\mathbf{M}$ can each contain up to n nonzero entries corresponding to the n JJ coefficients of $\mathbf{M}\boldsymbol{\Phi}_b$, whose magnitudes are equivalent in this work. The other m inductive elements of $\mathbf{M}$—corresponding to the inductive coefficients in each of these rows—will either be zero or proportional to C_L/C_J; for the latter case, their magnitudes are chosen to satisfy Eq. (11). Once this constraint is satisfied, the limit $C_L/C_J \to 0$ is taken.

(2) When $m - F > 0$, the last $m - F$ rows of $\mathbf{M}$ will each contain up to m nonzero entries corresponding to the m inductive flux coefficients of $\mathbf{M}\boldsymbol{\Phi}_b$: In each of these rows, the nonzero entries should be given magnitudes that satisfy Eq. (11). Meanwhile, each row's n JJ coefficients should have zero-valued entries.

Importantly, linear independence between rows must be maintained when implementing both these conditions.

To briefly illustrate guideline (1), one possible realization is that in each of the n rows, every JJ coefficient takes on a nonzero value only once, while all other JJ coefficients are zero. If each nonzero value is unity, then this is equivalent to a simple permutation between branch and irrotational flux coordinates.

Guideline (2) stems from a mismatch between the number of loops and inductors. For example, if $m = 2$ and $F = 1$ such that $m - F = 1$—i.e., there is one loop that contains more than one inductor—then this requires setting all JJ coefficients to zero for one solution of Eq. (11). This reflects the overdetermination of the additional inductor's behavior in the circuit. Consequently, one cyclic coordinate will appear in the circuit Lagrangian; this can be eliminated through determining its equation of motion and subsequently rewriting it in terms of noncyclic irrotational degrees of freedom. Sections IV A and IV B demonstrate this procedure. Note that if $m - F = 0$, then guideline (2) has no effect.
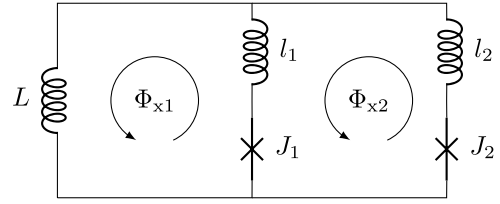

FIG. 1. A SQUID with $N = 5$ and $F = 2$. Slight adjustments are made to the physical construction of the circuit compared to Ref. [5].

Once the elements of $\mathbf{M}$ are determined, the dynamical degrees of freedom are interpreted as the irrotational degrees of freedom that are not cyclic [21]. Numerically, there are $N - F - (m - F) = n$ of them, as there will be $N - F$ irrotational flux coordinates with $m - F$ expected to be cyclic. For a multiloop circuit, i.e., $F > 1$, a diagonal $\mathbf{C}_{\mathrm{eff}}$ can only be found when there are at least as many irrotational degrees of freedom as JJs. In light of this, when dealing with multiloop circuits, we specialize to circuits that satisfy $N - F - n \geqslant 0$. Equivalently, we can say that the number of inductors in a multiloop circuit containing both JJs and inductors must satisfy $m \geqslant F$.

An example where $m - F < 0$ leads to a nondiagonal $\mathbf{C}_{\mathrm{eff}}$ can be found in the circuit in Sec. V B of Ref. [17], since the authors do not include an inductor in their $F = 2$ circuit. On the one hand, this means $m = 0 \ngeqslant 2$, i.e., a violation of the guidelines, resulting in a less-interpretable circuit Lagrangian. On the other hand, in Ref. [20], $m = 1$ while $F = 1$, which satisfies $m \geqslant F$; this led to experimentally verifying both the method of finding irrotational flux degrees of freedom and the implementation of the guidelines for their application of using their circuit construction to investigate energy eigenstates with their circuit's Hamiltonian.

IV. EXAMPLE SQUID DESIGNS

Now, we illustrate the procedures described above by working out two examples. Section IV A derives the circuit Lagrangian and equations of motion of a SQUID that contains two loops constructed by composing two well known SQUID designs: One loop containing one inductor and one Josephson junction—known as a radio-frequency SQUID [31–34]—while the other loop has two inductors and two Josephson junctions—known as a direct-current SQUID [6,33,35]. In Sec. IV B, we derive the potential of a device composed of two of these SQUIDs via mutual inductive coupling. Notably, the potential energy landscape for each example device can be readily used for classical information processing—see the Appendix for a brief overview.

A. SQUID

We first consider a circuit whose names and constructions span multiple use cases over a number of decades. Figure 1 displays a circuit whose original name was the variable β radio-frequency SQUID [4,5,10] and was later known as the compound Josephson junction radio-frequency SQUID [11,36]. The device's primary use cases involved investigating

macroscopic quantum phenomenon, which deviates fundamentally from our goals. Applications that utilize the quantum flux parametron (QFP) [9,13,14,37] align more closely with our goals—employing superconducting devices for classical information processing—although the QFP construction and methods of operation differ from that of Refs. [4,5,10]. With this considered, we refer to the circuit in Fig. 1 as a SQUID.

The goal is to reproduce the Lagrangian of the circuit shown in Fig. 1—whose design is detailed in Ref. [5]—using the methods detailed in Secs. III A and III B.

To accomplish this, we first begin writing out the flux vectors:

$$\mathbf{\Phi}_b = \begin{pmatrix} \phi_{J_1} & \phi_{J_2} & \phi_L & \phi_{l_1} & \phi_{l_2} \end{pmatrix}^\mathsf{T}, \tag{14}$$

$$\mathbf{\Phi}_{b_J} = \begin{pmatrix} \phi_{J_1} & \phi_{J_2} \end{pmatrix}^\mathsf{T}, \tag{15}$$

$$\mathbf{\Phi}_{b_L} = \begin{pmatrix} \phi_L & \phi_{l_1} & \phi_{l_2} \end{pmatrix}^\mathsf{T}, \tag{16}$$

$$\widetilde{\mathbf{\Phi}}_+ = \begin{pmatrix} \widetilde{\phi}_1 & \widetilde{\phi}_2 & \widetilde{\phi}_3 & \phi_{\mathrm{x}_1} & \phi_{\mathrm{x}_2} \end{pmatrix}^\mathsf{T}. \tag{17}$$

With every branch orientation in Fig. 1 pointing upwards, fluxoid quantization gives:

$$\mathbf{R} = \begin{pmatrix} 1 & 0 & -1 & 1 & 0 \\ -1 & 1 & 0 & -1 & 1 \end{pmatrix},$$

where each row's entries correspond to the column orientation of (J_1, J_2, L, l_1, l_2), and each row coincides with the external flux loops $(\phi_{\mathrm{x}_1}, \phi_{\mathrm{x}_2})$, respectively. Next, the capacitance matrix is written as:

$$\mathbf{C}^{-1} = \mathrm{diag}(C_{J_1}^{-1}, C_{J_2}^{-1}, C_L^{-1}, C_{l_1}^{-1}, C_{l_2}^{-1}).$$

To satisfy Eq. (11), let:

$$\mathbf{M}^\mathsf{T} = \begin{pmatrix} M_{11} & M_{21} & M_{31} \\ M_{12} & M_{22} & M_{32} \\ M_{13} & M_{23} & M_{33} \\ M_{14} & M_{24} & M_{34} \\ M_{15} & M_{25} & M_{35} \end{pmatrix}.$$

Then, with the assumption that $C_l := C_{l_1} = C_{l_2} = C_L$ and $C_J := C_{J_1} = C_{J_2}$, we enforce Eq. (11); Each column of $\mathbf{M}^\mathsf{T}$ satisfies:

$$CM_{i1} = M_{i3} - M_{i4} \tag{18}$$

$$C(M_{i2} - M_{i1}) = M_{i4} - M_{i5}, \tag{19}$$

with $C := C_l/C_J$ and i $= 1, 2, 3$. From here, we use the guidelines described in Sec. III B to obtain a diagonal $\mathbf{C}_{\mathrm{eff}}$. This is achieved first via guideline (1) for the first $n = 2$ rows of $\mathbf{M}$ and guideline (2) for the last $m - F = 1$ row of $\mathbf{M}$. We then write a subset of the solution space of Eqs. (18) and (19) into

the augmented matrix:

$$\mathbf{M}_+ = \begin{pmatrix} \mathbf{M} \\ \mathbf{R} \end{pmatrix}$$
$$= \begin{pmatrix} 1/2 & 1/2 & C/4 & -C/4 & -C/4 \\ -1 & 1 & 0 & C & -C \\ 0 & 0 & 1 & 1 & 1 \\ 1 & 0 & -1 & 1 & 0 \\ -1 & 1 & 0 & -1 & 1 \end{pmatrix}, \tag{20}$$

We expect there to be $N - F = 3$ irrotational degrees of freedom with $m - F = 1$ of them being cyclic once the circuit Lagrangian $\mathcal{L}$ is found. Next, taking the limit $C \to 0$ and then inverting $\mathbf{M}_+$ yields:

$$\mathbf{M}_+^{-1} = \begin{pmatrix} 1 & -1/2 & 0 & 0 & 0 \\ 1 & 1/2 & 0 & 0 & 0 \\ 2/3 & 0 & 1/3 & -2/3 & -1/3 \\ -1/3 & 1/2 & 1/3 & 1/3 & -1/3 \\ -1/3 & -1/2 & 1/3 & 1/3 & 2/3 \end{pmatrix}, \tag{21}$$

which aids in computing the effective capacitive matrix from Eq. (13) as:

$$\mathbf{C}_{\mathrm{eff}} = \begin{pmatrix} 2C_J & 0 & 0 & 0 & 0 \\ 0 & C_J/2 & 0 & 0 & 0 \\ 0 & 0 & 0 & 0 & 0 \\ 0 & 0 & 0 & 0 & 0 \\ 0 & 0 & 0 & 0 & 0 \end{pmatrix},$$

which is diagonal as expected due to following guidelines (1) and (2).

As there are no mutual inductance couplings, the inductance matrix is

$$\mathbf{L} = \begin{pmatrix} L & 0 & 0 \\ 0 & l_1 & 0 \\ 0 & 0 & l_2 \end{pmatrix}.$$

Recalling Eq. (10) and writing the circuit Lagrangian from Eq. (5) in terms of irrotational branch fluxes, produces:

$$\mathcal{L} = \frac{C_J}{2}\left(2\widetilde{\dot{\phi}}_1^2 + \frac{1}{2}\widetilde{\dot{\phi}}_2^2\right) - \frac{1}{9L}\left(2\widetilde{\phi}_1 + \widetilde{\phi}_3 - 2\phi_{x_1} - \phi_{x_2}\right)^2$$
$$- \frac{1}{9l_1}\left(-\widetilde{\phi}_1 + \frac{3}{2}\widetilde{\phi}_2 + \widetilde{\phi}_3 + \phi_{x_1} - \phi_{x_2}\right)^2$$
$$- \frac{1}{9l_2}\left(-\widetilde{\phi}_1 - \frac{3}{2}\widetilde{\phi}_2 + \widetilde{\phi}_3 + \phi_{x_1} + 2\phi_{x_2}\right)^2$$
$$+ E_{2+1}\cos\widetilde{\varphi}_1\cos\frac{\widetilde{\varphi}_2}{2} - E_{2-1}\sin\widetilde{\varphi}_1\sin\frac{\widetilde{\varphi}_2}{2}, \tag{22}$$

where $E_{2\pm1} = E_{J_2} \pm E_{J_1}$.

The Lagrangian is independent of $\widetilde{\dot{\phi}}_3$ indicating that it is, as expected, a cyclic degree of freedom: It can be eliminated by computing the Euler-Lagrange equation of motion and substituting. For ease of calculation, we use standard assumptions about the circuit inductance parameters from Ref. [5], $l := l_1 = l_2 \ll L$. With these assumptions, the Euler-Lagrange equations yield $\widetilde{\phi}_3 = \widetilde{\phi}_1 - \phi_{x_1} - \phi_{x_2}/2$ which we then substitute into $\mathcal{L}$. A map between the circuit flux

variables in Eq. (22) and those from Ref. [5] can then be identified as:

$$\widetilde{\phi}_1 = \phi, \qquad (23)$$

$$\widetilde{\phi}_2 = \phi_{\mathrm{dc}}, \qquad (24)$$

$$\phi_{x_1} = \phi_{\mathrm{x}} - \tfrac{1}{2}\phi_{\mathrm{xdc}}, \text{ and} \qquad (25)$$

$$\phi_{x_2} = \phi_{\mathrm{xdc}}. \qquad (26)$$

Making these substitutions into Eq. (22) yields a Lagrangian $\mathcal{L}$ that matches that of Ref. [5] with the preceding variable substitutions:

$$\mathcal{L} = \mathcal{L}_T - \mathcal{L}_{\mathrm{SQUID}} \qquad (27)$$

$$= \frac{C_J}{2}\left(2\dot{\phi}^2 + \frac{1}{2}\dot{\phi}_{\mathrm{dc}}^2\right) - \frac{1}{2L}(\phi - \phi_{\mathrm{x}})^2 - \frac{1}{4l}(\phi_{\mathrm{dc}} - \phi_{\mathrm{xdc}})^2$$

$$+ E_{2+1}\cos\varphi\cos\frac{\varphi_{\mathrm{dc}}}{2} - E_{2-1}\sin\varphi\sin\frac{\varphi_{\mathrm{dc}}}{2}.$$

The goal is to now obtain the full Langevin equation of motion in Eq. (9) for the circuit in Fig. 1. Since we wrote the circuit Lagrangian in Eq. (27) in terms of the coordinates ϕ and ϕ_{dc}, we now need to transform the dissipative contribution in Eq. (8) into the irrotational flux basis. Assuming both JJ shunts have a dc resistance of R, we have $\mathbf{D}^{-1} = \mathrm{diag}(1/R,\ 1/R)$. This leads to:

$$\mathcal{D} = \frac{1}{2}\dot{\boldsymbol{\Phi}}_{b_J}^{\mathsf{T}}\mathbf{D}^{-1}\dot{\boldsymbol{\Phi}}_{b_J}$$

$$= \frac{1}{2R}\left(\dot{\phi}_{J_1}^2 + \dot{\phi}_{J_2}^2\right). \qquad (28)$$

Now, we use $\mathbf{M}_+^{-1}$ from Eq. (21) to write the branch fluxes in terms of irrotational coordinates with the relation $\dot{\boldsymbol{\Phi}}_b = \mathbf{M}_+^{-1}\dot{\widetilde{\boldsymbol{\Phi}}}_+$ from Eq. (10):

$$\dot{\phi}_{J_{1,2}} = \dot{\widetilde{\phi}}_1 \mp \tfrac{1}{2}\dot{\widetilde{\phi}}_2 = \dot{\phi} \mp \tfrac{1}{2}\dot{\phi}_{\mathrm{dc}}, \qquad (29)$$

where the last equality was obtained using Eqs. (23) and (24). Further substituting this into the dissipation function yields:

$$\mathcal{D} = \frac{1}{R}\left(\dot{\phi}^2 + \frac{1}{4}\dot{\phi}_{\mathrm{dc}}^2\right). \qquad (30)$$

By using Eq. (9), we can write the Langevin equation of motion in terms of the dynamical variables ϕ and ϕ_{dc}:

$$2C_J\ddot{\phi} = -\frac{1}{L}(\phi - \phi_{\mathrm{x}}) - I_{\mathrm{c}2+\mathrm{c}1}\sin\varphi\cos\frac{\varphi_{\mathrm{dc}}}{2}$$

$$- I_{\mathrm{c}2-\mathrm{c}1}\cos\varphi\sin\frac{\varphi_{\mathrm{dc}}}{2} - \frac{2}{R}\dot{\phi} + \eta(t), \qquad (31)$$

$$\frac{C_J}{2}\ddot{\phi}_{\mathrm{dc}} = -\frac{1}{2l}(\phi_{\mathrm{dc}} - \phi_{\mathrm{xdc}}) - I_{\mathrm{c}2+\mathrm{c}1}\cos\varphi\sin\frac{\varphi_{\mathrm{dc}}}{2}$$

$$- I_{\mathrm{c}2-\mathrm{c}1}\sin\varphi\cos\frac{\varphi_{\mathrm{dc}}}{2} - \frac{1}{2R}\dot{\phi}_{\mathrm{dc}} + \eta_{\mathrm{dc}}(t). \qquad (32)$$

B. Inductively coupled SQUIDs

For our final example, consider inductively coupling two SQUIDs through L_1 and L_2 via the mutual inductance coupling constant $M := M_{12} = M_{21}$, shown in Fig. 2. Using the
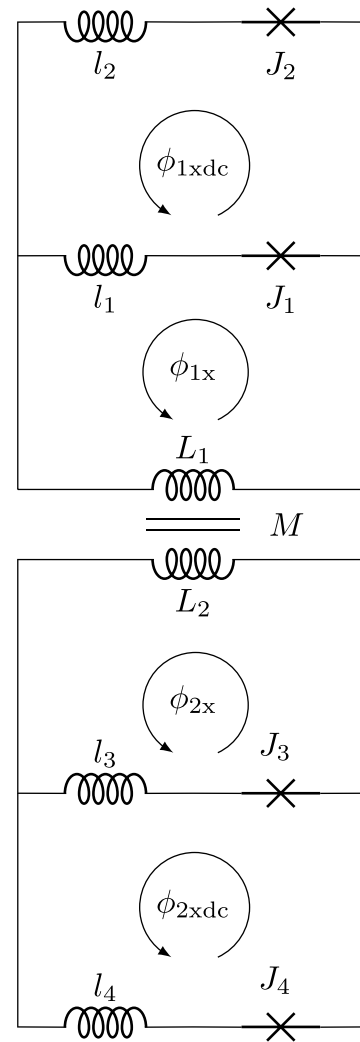

FIG. 2. Two SQUIDs inductively coupled via M: A superconducting device that supports two-bit classical computations through the manipulation of its potential energy landscape.

methods described in Secs. III A and III B, as well as the results from Sec. IV A, allows for rapidly deriving its potential in a more interpretable way.

The choice of branch orientation for the circuit in Fig. 2 is represented by:

$$\mathbf{R} = \begin{pmatrix} 1 & 0 & 0 & 0 & -1 & 0 & 1 & 0 & 0 & 0 \\ -1 & 1 & 0 & 0 & 0 & 0 & -1 & 1 & 0 & 0 \\ 0 & 0 & 1 & 0 & 0 & -1 & 0 & 0 & 1 & 0 \\ 0 & 0 & -1 & 1 & 0 & 0 & 0 & 0 & -1 & 1 \end{pmatrix},$$

in which each row's elements coincide with the column orientation $(J_1, J_2, J_3, J_4, L_1, L_2, l_1, l_2, l_3, l_4)$, each row corresponds to the external flux loop $(\phi_{1\mathrm{x}}, \phi_{1\mathrm{xdc}}, \phi_{2\mathrm{x}}, \phi_{2\mathrm{xdc}})$, and each branch orientation of the upper (lower) SQUID points left (right). Using the irrotational constraint $\mathbf{R}\mathbf{C}^{-1}\mathbf{M}^{\mathsf{T}} = \mathbf{0}$, we find that the elements of $\mathbf{M}$ need to satisfy:

$$CM_{\mathrm{i}1} = M_{\mathrm{i}5} - M_{\mathrm{i}7}$$

$$C(M_{\mathrm{i}2} - M_{\mathrm{i}1}) = M_{\mathrm{i}7} - M_{\mathrm{i}8}$$

$$CM_{i3} = M_{i6} - M_{i9}$$

$$C(M_{i4} - M_{i3}) = M_{i9} - M_{i10}.$$

Taking a lesson from the single SQUID case, and after taking $C \to 0$, our choice of **M** and **R** leads to:

$$\mathbf{M}_+ = \begin{pmatrix} 1/2 & 1/2 & 0 & 0 & 0 & 0 & 0 & 0 & 0 & 0 \\ -1 & 1 & 0 & 0 & 0 & 0 & 0 & 0 & 0 & 0 \\ 0 & 0 & 1/2 & 1/2 & 0 & 0 & 0 & 0 & 0 & 0 \\ 0 & 0 & -1 & 1 & 0 & 0 & 0 & 0 & 0 & 0 \\ 0 & 0 & 0 & 0 & 1 & 0 & 1 & 1 & 0 & 0 \\ 0 & 0 & 0 & 0 & 0 & 1 & 0 & 0 & 1 & 1 \\ & & & & & \mathbf{R} & & & & \end{pmatrix},$$

whose inverse is:

$$\mathbf{M}_+^{-1} = \begin{pmatrix} 1 & -1/2 & 0 & 0 & 0 & 0 & 0 & 0 & 0 & 0 \\ 1 & 1/2 & 0 & 0 & 0 & 0 & 0 & 0 & 0 & 0 \\ 0 & 0 & 1 & -1/2 & 0 & 0 & 0 & 0 & 0 & 0 \\ 0 & 0 & 1 & 1/2 & 0 & 0 & 0 & 0 & 0 & 0 \\ 2/3 & 0 & 0 & 0 & 1/3 & 0 & -2/3 & -1/3 & 0 & 0 \\ 0 & 0 & 2/3 & 0 & 0 & 1/3 & 0 & 0 & -2/3 & -1/3 \\ -1/3 & 1/2 & 0 & 0 & 1/3 & 0 & 1/3 & -1/3 & 0 & 0 \\ -1/3 & -1/2 & 0 & 0 & 1/3 & 0 & 1/3 & 2/3 & 0 & 0 \\ 0 & 0 & -1/3 & 1/2 & 0 & 1/3 & 0 & 0 & 1/3 & -1/3 \\ 0 & 0 & -1/3 & -1/2 & 0 & 1/3 & 0 & 0 & 1/3 & 2/3 \end{pmatrix}.$$

We then eliminate the cyclic degrees of freedom $\widetilde{\phi}_5$ and $\widetilde{\phi}_6$. Following the single SQUID case detailed in Sec. IV A, the map between our flux variables and those of Ref. [5] is as follows:

$$\widetilde{\phi}_i = \phi_j,$$

$$\widetilde{\phi}_{i+1} = \phi_{j\mathrm{dc}},$$

$$\phi_{x_i} = \phi_{jx} - \frac{1}{2}\phi_{jx\mathrm{dc}}, \text{ and}$$

$$\phi_{x_{i+1}} = \phi_{jx\mathrm{dc}}.$$

Here the index i corresponds to either the ith dynamical degree of freedom or the ith external flux, while the index j aligns with the flux in the jth SQUID, for which $i = 1, 3$ and $j = 1, 2$, respectively.

Next, the inductive contribution to the potential, when taking $L \coloneqq L_1 = L_2$ and $l \coloneqq l_1 = l_2 = l_3 = l_4$, is found by first writing:

$$\mathbf{L} = \begin{pmatrix} L & -M & 0 & 0 & 0 & 0 \\ -M & L & 0 & 0 & 0 & 0 \\ 0 & 0 & l & 0 & 0 & 0 \\ 0 & 0 & 0 & l & 0 & 0 \\ 0 & 0 & 0 & 0 & l & 0 \\ 0 & 0 & 0 & 0 & 0 & l \end{pmatrix}.$$

Then, subsequently taking its inverse gives:

$$\mathbf{L}^{-1} = \begin{pmatrix} 1/L_\alpha & \mu/L_\alpha & 0 & 0 & 0 & 0 \\ \mu/L_\alpha & 1/L_\alpha & 0 & 0 & 0 & 0 \\ 0 & 0 & 1/l & 0 & 0 & 0 \\ 0 & 0 & 0 & 1/l & 0 & 0 \\ 0 & 0 & 0 & 0 & 1/l & 0 \\ 0 & 0 & 0 & 0 & 0 & 1/l \end{pmatrix},$$

where $L_\alpha = \alpha L$, $\alpha = 1 - \mu^2$, and $\mu = M/L$.

With this, the potential is then:

$$\begin{aligned} \mathcal{L}_V = {} & -E_{2+1} \cos \varphi_1 \cos \frac{\varphi_{1\mathrm{dc}}}{2} + E_{2-1} \sin \varphi_1 \sin \frac{\varphi_{1\mathrm{dc}}}{2} \\ & - E_{4+3} \cos \varphi_2 \cos \frac{\varphi_{2\mathrm{dc}}}{2} + E_{4-3} \sin \varphi_2 \sin \frac{\varphi_{2\mathrm{dc}}}{2} \\ & + \frac{1}{4l}(\phi_{1\mathrm{dc}} - \phi_{1x\mathrm{dc}})^2 + \frac{1}{4l}(\phi_{2\mathrm{dc}} - \phi_{2x\mathrm{dc}})^2 \\ & + \frac{1}{2L_\alpha}(\phi_1 - \phi_{1x})^2 + \frac{1}{2L_\alpha}(\phi_2 - \phi_{2x})^2 \\ & + \frac{\mu}{L_\alpha}(\phi_1 - \phi_{1x})(\phi_2 - \phi_{2x}). \end{aligned} \tag{33}$$

If we assume small coupling by keeping only linear terms in μ, then $L_\alpha^{-1} \to L^{-1}$, resulting in Eq. (33) simplifying to a sum of two SQUIDs potential contributions and a mutual inductance coupling $\mathcal{L}_{\mathrm{M.I.}}$:

$$\mathcal{L}_V = \mathcal{L}_{\text{SQUID-1}} + \mathcal{L}_{\text{SQUID-2}} + \mathcal{L}_{\mathrm{M.I.}}, \tag{34}$$

in which $\mathcal{L}_{\mathrm{M.I.}} = \mu(\phi_1 - \phi_{1x})(\phi_2 - \phi_{2x})/L$. This Lagrangian can be used in much the same way as that in Eq. (27) to obtain the full equations of motion through Eq. (9).

V. CONCLUSION

We introduced a method that enables exploring the classical informational processing properties of a candidate superconducting circuit through understanding the circuit's energetics and subsequent dynamics. Through examples, we demonstrated the analytical efficiency of the method by reproducing the equations of motion for a SQUID that implements single-bit computations [12], as well as a more complicated device that supports two-bit computations.

This is the first effort in a series on physically realizable classical computing. In point of fact, the coupled SQUIDs shown in Fig. 2 also support the information processing behavior exhibited by a Szilard engine [1,38,39]. Follow-on efforts explore the dynamical and thermodynamic properties of these circuits and implement universal gates—e.g., NAND and Fredkin.

APPENDIX: COMPUTING WITH POTENTIAL ENERGY LANDSCAPES

Consider a potential energy landscape, generated by a physical substrate, that contains energy minima and is connected to a thermal environment that introduces damping and noise into the landscape's dynamics. The minima are separated by energy barriers whose heights are substantially larger than the thermal energy $k_B T$. The thermal environment quickly induces distributions of microstates to settle into local equilibria in the phase space regions surrounding the minima. Noise perturbs the microstates within these wells; however, it is unlikely to drive the microstates between these respective regions on a timescale that scales exponentially with the energy barrier height. Thus, the energy barriers prevent mixing between these wells except on these very long timescales. As a result, the minima serve to support long-lived mesoscopic system states—metastable memory states. Manipulating them with the potential's dynamics corresponds to information processing.

Armed with the potential energy surfaces corresponding to Eqs. (27) and (34), we can choose parameter values which give rise to controllable metastable memory states; Fig. 3 displays these landscapes. The reasoning behind these choices, as well as an outline for how one-bit and two-bit computations are performed via external circuit parameter modifications, are detailed here in the Appendix.

1. Double well potential

To carry out one-bit computations with Eq. (27)—which is generated by the single SQUID in Fig. 1—we make the following choices in line with the superconducting circuit literature [5,12,40]: $E_{2+1} = 1.05 \times 10^{-21}$ J, while $E_{2-1} = 0$. The latter assumption gives symmetry to the potential. We also set $L = 230$ pH [40].

After implementing these selections, Eq. (27) produces the potential shown in Fig. 3(a). Here the potential has neutral external parameter values, i.e., $\varphi_{xdc} = \varphi_x = 0$. The potential
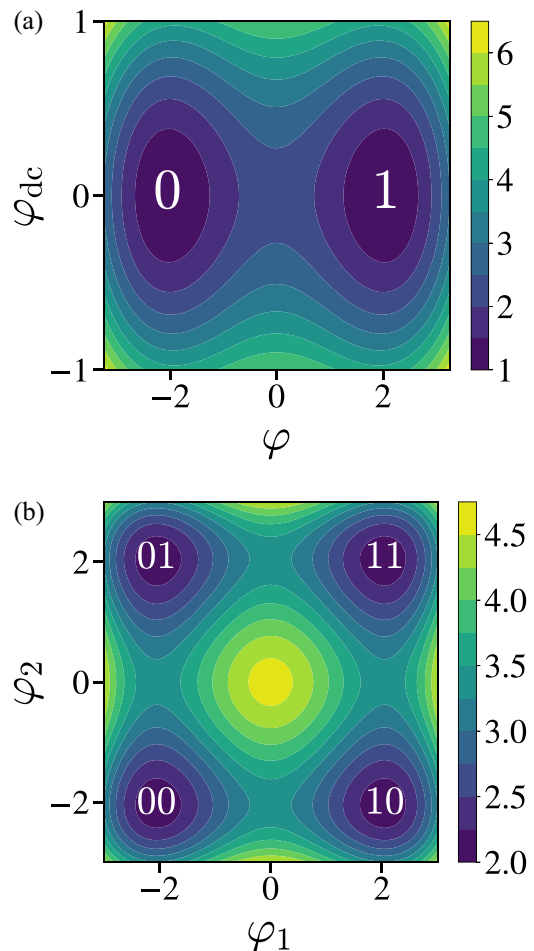

FIG. 3. Potential energy landscapes generated by parameter values specifically chosen for the application of performing computations. (a) The double well potential—a landscape representing one bit of information—which can be generated by Eq. (27). By changing the value of φ_x and φ_{xdc}, one-bit computations can be carried out [12,26]. (b) The quadruple well potential generated by Eq. (34). Modifying μ, φ_{ix}, and φ_{ixdc}, for $i = 1, 2$, can lead to performing two-bit computations.

contains two stable energy minima separated by a large energy barrier—i.e., two metastable memory states. We choose to assign computational memory states to each minima based on their location with respect to the φ axis:

$$\text{state} = \begin{cases} 0 & \text{if} \quad \varphi < 0, \\ 1 & \text{if} \quad \varphi > 0. \end{cases} \quad \text{(A1)}$$

Double well potentials provide a platform for studying one-bit operations; for example, Landauer [3] in 1961 used it to study the minimum heat dissipation due to irreversible information erasure. Previous works have investigated SQUID-generated double well potentials for their nonequilibrium thermodynamic properties [4,10]; one-bit erasure operations [12]; one-bit swaps [26]; and other classical information processing applications [9,14,37], including at the microprocessor scale [13].

2. Quadruple well potential

One way of carrying out two-bit computations with the potential in Eq. (34) is to reduce it to an effective two-dimensional surface of interest. Accomplishing this can be done by making the following assumptions that are analogous to the one-bit case in Sec. A 1: First, $E_{2+1} = E_{4+3} = 1.05 \times 10^{-21}$ J [40], while $E_{2-1} = E_{4-3} = 0$. Importantly, we assume $l \ll L = 230$ pH; this assumption means that changes in φ_{ixdc} will be reflected in φ_{idc} on short enough timescales for $i = 1, 2$. Because of this, we assume $\varphi_{idc} = \varphi_{ixdc}$, and Eq. (34) is reduced to the effective two-dimensional potential energy surface in the $\varphi_1 - \varphi_2$ plane shown in Fig. 3(b). Here the external parameter values are zero-valued, i.e., $\varphi_{1xdc} = \varphi_{2xdc} = 0$ and $\mu = 0$. This potential contains four stable wells that can each be assigned a computational memory state—00, 01, 10, and 11. The ordering of these memory states in the potential is arbitrarily chosen by a minimum's location with respect to the $\varphi_1 - \varphi_2$ axis:

$$\text{first (second) bit} = \begin{cases} 0 & \text{if } \varphi_1 \, [\varphi_2] < 0, \\ 1 & \text{if } \varphi_1 \, [\varphi_2] > 0. \end{cases} \quad \text{(A2)}$$

By varying the values of M, φ_{ix}, and φ_{ixdc} for which $i = 1, 2$, we can process that information—using the dynamics of the Euler-Lagrange equation of motion via Eq. (9) to implement two-bit logic gates. Note that while we considered M to be a tunable coupling constant, the details of its construction—a SQUID coupler—are detailed in Refs. [36,41,42]. The coupler's equations of motion could be accounted for within the complete device construction if its dynamics become important in future investigations.

[1] A. B. Boyd and J. P. Crutchfield, Maxwell demon dynamics: Deterministic chaos, the Szilard map, and the intelligence of thermodynamic systems, Phys. Rev. Lett. **116**, 190601 (2016).

[2] K. J. Ray, A. B. Boyd, G. W. Wimsatt, and J. P. Crutchfield, Non-Markovian momentum computing: Thermodynamically efficient and computation universal, Phys. Rev. Res. **3**, 023164 (2021).

[3] R. Landauer, Irreversibility and heat generation in the computing process, IBM J. Res. Dev. **5**, 183 (1961).

[4] S. Han, J. Lapointe, and J. E. Lukens, Thermal activation in a two-dimensional potential, Phys. Rev. Lett. **63**, 1712 (1989).

[5] S. Han, J. Lapointe, and J. E. Lukens, Variable ß rf SQUID, in *Single-Electron Tunneling and Mesoscopic Devices* (Springer, Berlin, 1992), vol. 31, pp. 219–222.

[6] R. Cantor, Dc SQUIDs: Design, optimization and practical applications, in *SQUID Sensors: Fundamentals, Fabrication and Applications* (Springer, Netherlands, Dordrecht, 1996), pp. 179–233.

[7] T. P. Orlando, J. E. Mooij, L. Tian, C. H. van der Wal, L. S. Levitov, S. Lloyd, and J. J. Mazo, Superconducting persistent-current qubit, Phys. Rev. B **60**, 15398 (1999).

[8] M. Mück, B. Chesca, and Y. Zhang, Radio frequency SQUIDs and their applications, in *Microwave Superconductivity* (Springer, Netherlands, Dordrecht, 2001), pp. 505–540.

[9] Y. Harada, E. Goto, and N. Miyamoto, Quantum flux parametron, in *1987 International Electron Devices Meeting* (1987), pp. 389–392.

[10] S. Han, J. Lapointe, and J. E. Lukens, Effect of a two-dimensional potential on the rate of thermally induced escape over the potential barrier, Phys. Rev. B **46**, 6338 (1992).

[11] R. Harris, M. W. Johnson, S. Han, A. J. Berkley, J. Johansson, P. Bunyk, E. Ladizinsky, S. Govorkov, M. C. Thom, S. Uchaikin, B. Bumble, A. Fung, A. Kaul, A. Kleinsasser, M. H. S. Amin, and D. V. Averin, Probing noise in flux qubits via macroscopic resonant tunneling, Phys. Rev. Lett. **101**, 117003 (2008).

[12] O.-P. Saira, M. H. Matheny, R. Katti, W. Fon, G. Wimsatt, J. P. Crutchfield, S. Han, and M. L. Roukes, Nonequilibrium thermodynamics of erasure with superconducting flux logic, Phys. Rev. Res. **2**, 013249 (2020).

[13] C. L. Ayala, T. Tanaka, R. Saito, M. Nozoe, N. Takeuchi, and N. Yoshikawa, MANA: A monolithic adiabatic integration architecture microprocessor using 1.4-zJ/op unshunted superconductor Josephson junction devices, IEEE J. Solid-State Circuits **56**, 1152 (2021).

[14] N. Takeuchi, T. Yamae, C. Ayala, H. Suzuki, and N. Yoshikawa, Adiabatic quantum-flux-parametron: A tutorial review, IEICE Trans. Electron. **E105.C**, 251 (2022).

[15] M. H. Devoret, *Quantum Fluctuations in Electrical Circuits* (Elsevier Science, Les Houches, Session LXIII, 1995).

[16] G. Burkard, R. H. Koch, and D. P. DiVincenzo, Multilevel quantum description of decoherence in superconducting qubits, Phys. Rev. B **69**, 064503 (2004).

[17] X. You, J. A. Sauls, and J. Koch, Circuit quantization in the presence of time-dependent external flux, Phys. Rev. B **99**, 174512 (2019).

[18] M. Mariantoni, The energy of an arbitrary electrical circuit, classical and quantum, arXiv:2007.08519.

[19] S. E. Rasmussen, K. S. Christensen, S. P. Pedersen, L. B. Kristensen, T. Baekkegaard, N. J. S. Loft, and N. T. Zinner, Superconducting circuit companion–an introduction with worked examples, PRX Quantum **2**, 040204 (2021).

[20] J. Bryon, K. K. Weiss, X. You, S. Sussman, X. Croot, Z. Huang, J. Koch, and A. A. Houck, Time-dependent magnetic flux in devices for circuit quantum electrodynamics, Phys. Rev. Appl. **19**, 034031 (2023).

[21] H. Goldstein, C. P. Poole, and J. L. Safko, *Classical Mechanics*, 3rd ed. (Addison-Wesley, San Francisco, 2008).

[22] M. Xiang-Guo, W. Ji-Suo, Z. Yun, and F. Hong-Yi, Number-phase quantization and deriving energy-level gap of two LC circuits with mutual-inductance, Chin. Phys. Lett. **25**, 1205 (2008).

[23] M. Xiang-Guo, W. Ji-Suo, and L. Bao-Long, Cooper-pair number-phase quantization for inductance coupling circuit including Josephson junctions, Chin. Phys. Lett. **25**, 1419 (2008).

[24] S. P. Chitta, T. Zhao, Z. Huang, I. Mondragon-Shem, and J. Koch, Computer-aided quantization and numerical analysis of superconducting circuits, New J. Phys. **24**, 103020 (2022).

[25] J. Ulrich and F. Hassler, Dual approach to circuit quantization using loop charges, Phys. Rev. B **94**, 094505 (2016).

[26] K. J. Ray and J. P. Crutchfield, Gigahertz sub-Landauer momentum computing, Phys. Rev. Appl. **19**, 014049 (2023).

[27] R. P. Riwar and D. P. DiVincenzo, Circuit quantization with time-dependent magnetic fields for realistic geometries, npj Quantum Inf. **8**, 36 (2022).

[28] W. C. Stewart, Current-voltage characteristics of Josephson junctions, Appl. Phys. Lett. **12**, 277 (1968).

[29] D. E. McCumber, Effect of ac impedance on dc voltage-current characteristics of superconductor weak-link junctions, J. Appl. Phys. **39**, 3113 (1968).

[30] B. Yurke and J. S. Denker, Quantum network theory, Phys. Rev. A **29**, 1419 (1984).

[31] J. E. Zimmerman, P. Thiene, and J. T. Harding, Design and operation of stable rf-biased superconducting point-contact quantum devices, and a note on the properties of perfectly clean metal contacts, J. Appl. Phys. **41**, 1572 (1970).

[32] J. M. Goodkind and D. L. Stolfa, The superconducting magnetic flux detector, Rev. Sci. Instrum. **41**, 799 (1970).

[33] A. Barone and G. Paternò, *Physics and Applications of the Josephson Effect* (Wiley, New York, 1982).

[34] J. Clarke, Principles and applications of SQUIDs, Proc. IEEE **77**, 1208 (1989).

[35] R. C. Jaklevic, John Lambe, A. H. Silver, and J. E. Mercereau, Quantum interference effects in Josephson tunneling, Phys. Rev. Lett. **12**, 159 (1964).

[36] R. Harris, T. Lanting, A. J. Berkley, J. Johansson, M. W. Johnson, P. Bunyk, E. Ladizinsky, N. Ladizinsky, T. Oh, and S. Han, Compound Josephson-junction coupler for flux qubits with minimal crosstalk, Phys. Rev. B **80**, 052506 (2009).

[37] M. Hosoya, W. Hioe, J. Casas, R. Kamikawai, Y. Harada, and Y. Wada, Quantum flux parametron: A single quantum flux device for Josephson supercomputer, IEEE Trans. Appl. Supercond. **1**, 77 (1991).

[38] L. Szilard, Über die ausdehnung der phänomenologischen thermodynamik auf die schwankungserscheinungen, Z. Phys. **32**, 753 (1925).

[39] L. Szilard, On the decrease of entropy in a thermodynamic system by the intervention of intelligent beings, Behav. Sci. **9**, 301 (1964).

[40] I. Ozfidan, C. Deng, A. Y. Smirnov, T. Lanting, R. Harris, L. Swenson, J. Whittaker, F. Altomare, M. Babcock, C. Baron, A. J. Berkley, K. Boothby, H. Christiani, P. Bunyk, C. Enderud, B. Evert, M. Hager, A. Hajda, J. Hilton, and S. Huang, Demonstration of a nonstoquastic Hamiltonian in coupled superconducting flux qubits, Phys. Rev. Appl. **13**, 034037 (2020).

[41] A. Maassen van den Brink, A. J. Berkley, and M. Yalowsky, Mediated tunable coupling of flux qubits, New J. Phys. **7**, 230 (2005).

[42] R. Harris, A. J. Berkley, M. W. Johnson, P. Bunyk, S. Govorkov, M. C. Thom, S. Uchaikin, A. B. Wilson, J. Chung, E. Holtham, J. D. Biamonte, A. Yu. Smirnov, M. H. S. Amin, and Alec Maassen van den Brink, Sign- and magnitude-tunable coupler for superconducting flux qubits, Phys. Rev. Lett. **98**, 177001 (2007).